Precision Agriculture (2026) 27:88
https://doi.org/10.1007/s11119-026-10391-0

Ground truth sampling methods affect accuracy of UAV-based vineyard yield estimation: a case study

Marco Canicattì[1,2] · Pietro Catania[1] · Eliseo Roma[1] · Salvatore Amato[1] · Massimo Vincenzo Ferro[1] · Mariangela Vallone[1] · Santo Orlando[1]

Received: 5 November 2025 / Accepted: 15 May 2026

Abstract

Purpose Accurate ground-truth data are essential for training reliable remote sensing (RS) models for vineyard yield estimation. However, previous UAV-based studies have mainly relied on single-vine sampling, which can introduce geometric inconsistencies due to canopy overlaps, vine spacing, and pruning configuration in Vertical Shoot Positioning (VSP) systems. This study aimed to assess how the choice of ground-truth sampling method, vine-based versus meter-based, affects the accuracy and robustness of UAV-derived yield models.

Methods UAV multispectral imagery was acquired at two phenological stages, BBCH 73 and BBCH 85, over a commercial vineyard trained to a VSP system. Yield data were collected using two ground-truth approaches, a vine-based method, recording the grape fresh weight per vine, and a meter-based method, measuring yield along contiguous one-meter canopy segments. UAV images were processed to derive spectral (NDVI) and geometric (fraction canopy cover, Fc) variables. Three estimation frameworks were evaluated: (*i*) linear regression models; (ii) machine learning algorithms (Efficient Linear, Support Vector Machine, Random Forest, and Gaussian Process Regression); and (iii) a Bayesian inference model.

Results Across all frameworks, the meter-based sampling approach outperformed the vine-based one. Linear regressions yielded higher determination coefficients (R^2=0.78) and lower nRMSE. ML algorithms achieved R^2 between 0.70 and 0.76 for meter-based sampling versus 0.15–0.27 for vine-based sampling. Bayesian model trained on meter-based sampled data demonstrated the highest predictive accuracy, achieving an R^2 of 0.84 with an nRMSE of 20.47% and a mean absolute error of 17.46%. In contrast, the model trained on vine-level data exhibited markedly lower performance ($R^2 = 0.41$, nRMSE = 50.08%). At the field scale, the meter-based sampling strategy, when coupled with Bayesian inference, delivered high-fidelity yield estimates with reduced posterior uncertainty.

Conclusion Ground-truth sampling design significantly affected UAV-based vineyard yield estimation. Sampling contiguous canopy segments preserves spatial continuity and mitigates geometric bias, enhancing model transferability and reliability across analytical frameworks. This approach provides a robust methodological foundation for scalable RS-based yield modelling in VSP vineyards.

Extended author information available on the last page of the article

Published online: 28 May 2026

Keywords Remote sensing · Bayesian inference · Uncertainty quantification · Precision viticulture · Multispectral imagery

Introduction

Grapes are one of the most widely grown fruit crops in the world, and environmental conditions, the physiological state of the plants and management practices can greatly influence grape yield and quality (Matese & Di Gennaro, 2015). In recent years, technological advances have introduced new tools to support this sector, giving rise to the concept of precision viticulture (PV). PV is based on the analysis, interpretation and management of spatial and temporal variability with the aim of optimising agronomic efficiency, improving economic and environmental sustainability (Matese and Di Gennaro 2015; Ferro et al. 2023a).

Recent advances in remote sensing (RS) techniques offer a valuable and efficient tool for monitoring vines at different scales. Among the various RS platforms, satellites and unmanned aerial vehicles (UAVs) are currently widely used and offer clear advantages for plant growth and health assessment (Di Gennaro et al. 2019a; Bollas et al. 2021). While satellite-based imagery provides valuable insights at the field and regional scales, its spatial resolution can be insufficient to capture the plant-scale variability in small and/or fragmented fields (Matese et al., 2017; Khaliq et al., 2019). As a complementary technology, UAVs enable rapid acquisition of ultra–high-resolution data at low operational costs and offer great flexibility in terms of flight scheduling and sensor integration (Mogili & Deepak, 2018; Canicattì & Vallone, 2024). Multispectral cameras capture reflectance signatures across spectral regions, enabling the extraction of biophysical information using vegetation indices (VI). Normalised difference vegetation index (NDVI), in particular, is widely used as a proxy of vigour and health status evaluation of a wide range of crops, including vineyard (Rouse et al. 1974a, b; Bannari et al. 1995; Xie et al. 2014). UAV-based multispectral imagery further enhanced vineyard canopies monitoring by enabling precise delineation of grapevine vegetation from background (i.e. weeds, soil and canopy's shadows) (Campos et al., 2014; Towers & Poblete-Echeverría, 2021). These tasks are increasingly supported by machine learning (ML) and deep learning (DL) algorithms for classification and segmentation of images (Cinat et al., 2019; Hossain & Chen, 2019; Pádua et al., 2022). Canopies detection allows the extraction of a spectral and geometrical features (Comba et al. 2020; Biglia et al. 2022; Catania et al. 2023b). Geometric features include canopy area (CA), thickness, canopy volume and fraction cover (Fc) (Campos et al. 2021a). The latter feature represents the ratio between canopy area and the available space per vine and has gained relevance in vineyard management. It is increasingly employed to support agronomic decisions, guide irrigation strategies, and serve as a key input for crop simulation models (Gao et al., 2020; Berry et al., 2024; Roma et al., 2025). Accurate estimation of vineyard yield is a key requirement for efficient harvest planning, logistical organization, and grape quality forecasting. However, yield estimation remains a challenging process due to the strong spatial and temporal variability of vine canopies and the practical constraints associated with field data collection. These limitations restrict the number of sampling sites that can be monitored within a vineyard (Guilpart et al., 2014; Júnior et al., 2018).

Traditionally, yield has been determined through manual measurements of the number of clusters, berries per cluster and average berry weight, with results typically expressed per vine or per unit area (Fuente et al., 2015; Araya-Alman et al., 2019). However, these measurements are subject to counting errors, particularly under dense canopies, and are influenced by marked intra- and inter-vine variability, as cluster weight may strongly differ even within the same vine (Clingeleffer & Krstic, 2003). From a statistical standpoint, an optimal sampling protocol should represent spatial distribution and variability in the vineyard population.

Since canopy architecture and physiological processes vary across space and time (Ferro et al. 2023a), sampling strategies must be designed to capture this embedded heterogeneity. Over the years, vineyard sampling methodologies have evolved from random to spatially informed approaches that account for within-field variability. Designs such as the randomized complete block (RCBD) and spatially balanced complete block (SBCB) have been developed to ensure a more uniform distribution of sampling points and to reduce the influence of underlying spatial gradients (Bramley & Hamilton, 2004; Acevedo-Opazo et al., 2010; Schoedl et al., 2012). The concept of spatial balance has since been extended to integrate RS data, including VIs and canopy structural metrics. This integration has proven effective in optimizing sample size, reducing it by up to 69%, and in minimizing travel distance during field surveys by up to 90%, without compromising accuracy (Meyers et al., 2011; Meyers & Vanden Heuvel, 2014). More recently, the use of management zones defined by yield variability or VIs has emerged as an efficient and statistically robust approach in PV (Squeri et al., 2021; Laurent et al., 2021; Valente et al., 2024).

Parallel to these advances in sampling design, numerous studies have investigated the use of UAV-based RS for vineyard yield estimation. Ballesteros et al. (2020a) achieved high prediction accuracy (RMSE = 0.5 kg·vine^{-1}; RE = 12.1%) by combining VIs and Fc metrics in a bilateral cordon system. Di Gennaro et al. (2019b) obtained over 84% accuracy in yield prediction through automated cluster detection on RGB imagery, while Leolini et al. (2023) and Lopez-García et al. (2022) reported RMSE values ranging from 0.21 to 0.39 kg·vine^{-1} in vineyards with different pruning systems. Although these studies confirm the potential of UAV imagery for accurate yield estimation, their reliance on vine-based ground-truth data limits the generalization of models across diverse vineyard architectures. Expressing yield per meter of canopy (kg·m^{-1}) rather than per vine provides a geometry-independent and spatially consistent reference, particularly suitable where canopy forms a continuous wall. This metric aligns more effectively with the spatial resolution of UAV imagery, where each pixel represents a portion of continuous vegetation, and minimizes the influence of vine spacing, pruning system, and canopy geometry. In previous studies, ground-truth datasets were typically derived from single-vine measurements, an approach that can introduce geometric inconsistencies in Vertical Shoot Positioning (VSP) systems due to the mismatch between the canopy structure, composed by interactions and overlaps between adjacent vines, and its two-dimensional projection on orthomosaics. The extent of this misalignment varies with canopy density, vigour, and training system, but some spatial inaccuracy is unavoidable when individual vines are used as discrete sampling units. In contrast, canopy-segment-based sampling mitigates these distortions, providing a more coherent framework for developing scalable and generalizable UAV-based yield models.

In this context, our hypothesis was that to modify the ground-truth sampling strategy, from a vine-based to a meter-based approach, can significantly influence the accuracy of the functional relationships between RS-derived variables and yield. Accordingly, the aim of this study was to compare two ground-based sampling methods for yield data collection in VSP-trained vineyards and to assess their impact on the predictive performance in different frameworks. Three analytical frameworks were investigated, including conventional linear correlation models, ML algorithms comprising Efficient Linear, Support Vector Machine, Random Forest, and Gaussian Process Regression, and a Bayesian inference framework.

Materials and methods

Experimental field description

The research was conducted during the growing season 2025 in an experimental site located in the Alcamo Protected Designation of Origin (PDO), in Sicily region (Fig. 1) (Italy, 37.92° N, 13.07° E; EPSG:4326) at an elevation of approximately 315 m a.s.l.). The area is characterized by a typical Mediterranean climate (Köppen, 1936), with mild, wet winters and hot and dry summers. Historical climatic data indicate a mean annual temperature of 19 °C, with average monthly maxima reaching 31.4 °C in August and minima occurring in Janu-

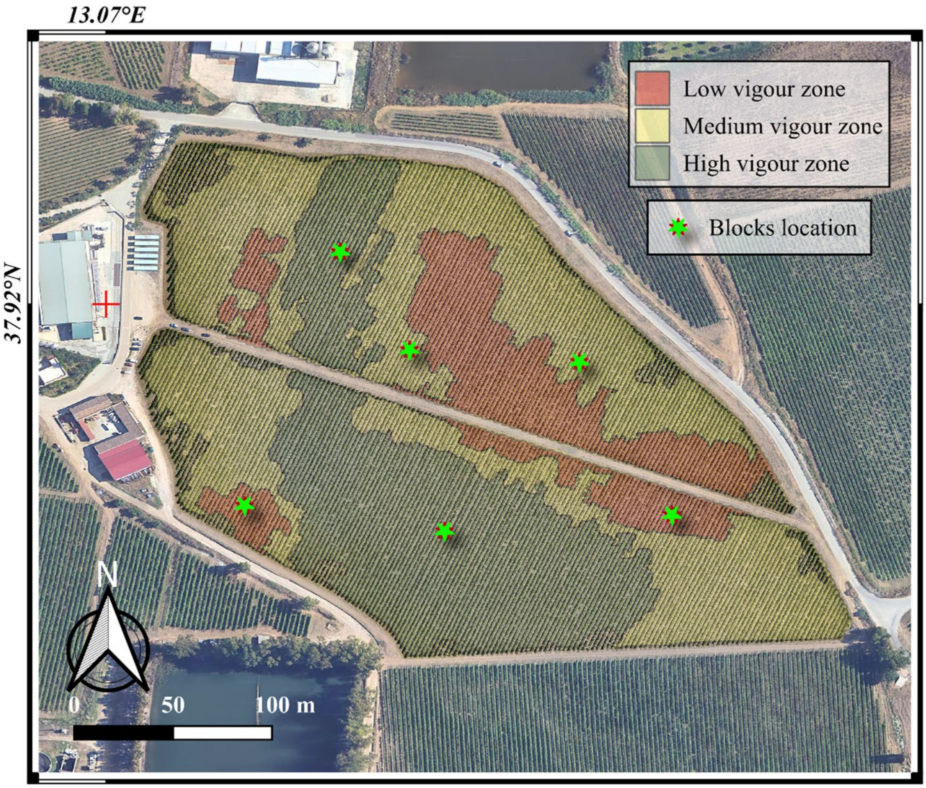

Fig. 1 Experimental field location (37.92° N, 13.07° E; EPSG:4326). Vigour zones are shown as low (red), medium (yellow), and high (green). Green stars indicate the positions of the sampling blocks groups within the vineyard (Color figure online)

ary. The mean annual precipitation is approximately 620–650 mm, most of which occurs between autumn and early spring.

The site is characterized by a gently sloping terrain, with gradients not exceeding 12%, and covers a total area of 7.6 ha. The vineyard was planted in 2007 with *Vitis vinifera* L. cv. Catarratto, grafted onto 1103 Paulsen rootstock. Vines are trained to a VSP system and pruned to a bilateral spur cordon, maintaining two buds per spur spaced at approximately 0.20 m. The planting layout follows a 2.20 inter-row × 1.00 m intra-row spacing, corresponding to a vine density of 4,545 vines ha^{-1}. The rows are oriented northeast–southwest (NE–SW), forming an angle of about 22° with respect to true north. The vineyard is managed under organic viticulture protocols, following ordinary agronomic and phytosanitary practices. Cultural operations include the application of composted manure, manual shoot positioning and pruning, and integrated pest management through sexual confusion techniques combined with the distribution of copper and sulphur-based treatments. Soil management consists of approximately five shallow tillage operations per year (to a depth of 0.10 m), aimed at controlling weeds, limiting surface evaporation, and preventing soil cracking. Nutrient inputs and plant protection measures were applied uniformly across the vineyard according to regional viticultural recommendations, ensuring balanced vegetative growth and high-quality fruit development. The site is equipped with a drip irrigation system, delivering an average seasonal water volume of approximately 600 m^3 ha^{-1} during the growing season to mitigate water stress under summer drought conditions.

Ground truth sampling methods

To appropriately capture the spatial variability within the experimental field and select the sampling locations, a comprehensive multisource spatial analysis was carried out.

Following the approach proposed by Canicattì et al. (2025a), multiple layers of historical information, collected between 2016 and 2025, were combined. Specifically, NDVI maps from Sentinel-2 satellite missions, were downloaded from the Copernicus Open Access Hub (ESA, https://browser.dataspace.copernicus.eu/). The time series was normalised and the per-pixel temporal standard deviation computed. Unstable areas were defined as pixels whose standard deviation exceeded the 80th percentile of the field-level distribution. Finally, a Jenks natural-breaks classification was applied to stable areas to partition the field into zones with consistent low, medium, and high vigour.

The areas identified by this approach were further validated by expert agronomic assessment and by multiple UAV-based multispectral surveys conducted between the 2021 and 2025.

Within each identified vigour zone, six spatially adjacent sampling blocks were delineated, this configuration was then replicated twice across the field, resulting in a total of 36 sampling blocks (3 vigour levels × 6 blocks × 2 replicates).

The field sampling procedure was designed to characterize yield components relative to both per-meter and per-vine units (Fig. 2). Specifically, two parallel spatial reference systems were established: one aligned with the projection of individual vines on the ground (Vine-based sampling unit), and one aligned with one-meter intervals along the row (Meter-based sampling unit).

For each delineated sampling segment, yield attributes were systematically collected. Specifically, the total fresh weight (defined here as yield), expressed as $kg{\cdot}m^{-1}$ or $kg{\cdot}vine^{-1}$,

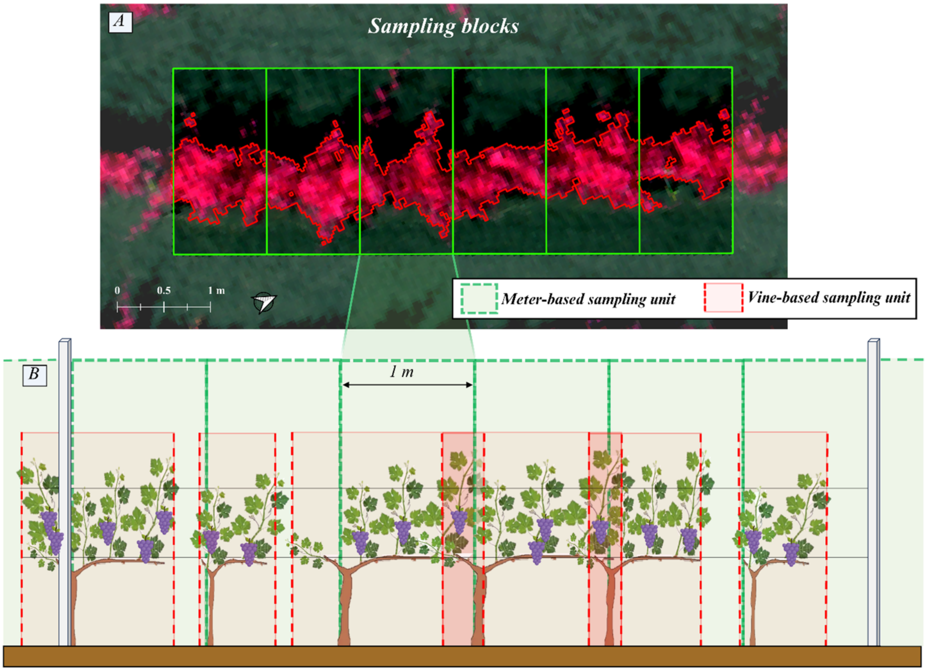

Fig. 2 Ground truth sampling design adopted in the vineyard. Sampling blocks configuration (**A**) and two sampling units (**B**) representation: (i) the vine-based sampling unit (red dashed lines), where measurements and yield components were collected individually for each vine, and (ii) the meter-based sampling unit (green dashed lines), corresponding to one-meter segments along the vine row (Color figure online)

was measured using a calibrated field scale, and the number of grape bunches (expressed as bunches per meter or per vine) was counted and recorded. Sampling was conducted sequentially along the rows to ensure a consistent representation of yield transitions across adjacent vines and block boundaries. The procedure began with the first vine of the first block, where production immediately outside the block boundary was harvested, followed by the yield inside the block from the first vine, potentially extending to part of the second vine, and then including the production of the first vine of the next block. This method ensured that each vine-meter encompassed four spatial contexts (outside, inside, overlapping, and adjacent). Once recorded data were processed to group the production at vine level and at the meter level.

UAV-based multispectral data acquisition and processing

The aerial surveys were conducted using a quadcopter system DJI Mavic 3 Multispectral (DJI, Shenzhen, China). The platform was equipped with a multispectral imaging system consisting of five sensors: one RGB (20 MP, 1/2″ CMOS) and four monochromatic bands covering green (550 ± 16 nm), red (660 ± 14 nm), red-edge (735 ± 10 nm), and near-infrared (NIR, 790 ± 22 nm) wavelengths, each with 5 MP resolution. All sensors were mounted on a 3-axis stabilized gimbal to ensure image stability during flight operations. To achieve high precision georeferencing, the UAV was equipped with an onboard GNSS mobile receiver, using RTK (real time kinematic). This configuration minimizes spatial errors in subsequent photogrammetric processing and VIs calculations. Data acquisition was performed around solar noon (12:30–13:30 local time) under optimal illumination conditions (clear sky, solar zenith angle < 30°).

Flight operations were conducted on May 23 and August 5, corresponding to the phenological stages of BBCH 73 and 85 respectively. In particular, the flight at BBCH 85, corresponding to the late ripening stage, was conducted shortly preceding harvest, whereas BBCH 73 correspondent to the onset of the berry growth stage, shortly after the end of flowering. These periods were selected as they represent two key windows for yield estimation in vineyards: a mid-season stage when the full vegetative development has already established, and a late-season stage when canopy condition closely reflect the final yield (Ballesteros et al. 2020b; López-García et al. 2022; Ferro et al. 2023b). The flight mission was planned using DJI Terra software (DJI, Shenzhen, China), with the following parameters. The UAV was operated at an altitude of 70 m above ground level (AGL), achieving a spatial resolution of 3.1 cm/pixel for multispectral imagery. Image acquisition used 75% frontal overlap and 70% side. The flight speed maintained at 3.2 m/s to optimize both operational efficiency and image quality. The flight path was set diagonally across the rows to improve the 3D reconstruction of the canopy and the orthomosaic reconstruction (Catania et al. 2023a). The multispectral imagery was processed using Agisoft Metashape Professional ver. 1.7.3 as photogrammetric software (Agisoft LLC, St. Petersburg, Russia). Image calibration was performed by placing a white Spectralon panel on the ground and the sunlight sensor of drone. The panel reflectance was measured immediately before and after the flight using a spectroradiometer (Fieldspec2). Before the flights some Ground Control Points (GCPs) were uniformly distributed and georeferenced in the field. This step ensured high precision georeferencing of the multispectral imagery.

The Fc and NDVI were evaluated for each poligon, corresponding to a vineyard block of 1 m in length al 2 m large. The positions of individual block and the boundaries of each block were georeferenced in the field using a Stonex S70 GPS receiver (Stonex S.r.l., Milan, Italy) and subsequently imported into QGIS ver. 3.36 (2023) to delimit the vines and blocks selected for the study.

Vineyard canopy pixels were isolated using a deep learning–based semantic segmentation approach. Specifically, a U-Net architecture with a ResNet-101 encoder backbone was implemented in PyTorch (Paszke et al., 2019), following the methodology described by Ferro et al. (2024). The encoder was initialized with ImageNet pre-trained weights to enhance feature extraction and accelerate convergence through transfer learning.

Prior to model training, multispectral imagery underwent radiometric correction and scaling to ensure consistency across all spectral bands. The input data consisted of radiometrically corrected surface reflectance values derived from the UAV imagery. These values were stored as 16-bit unsigned integers and converted to 32-bit floating-point format. Reflectance values were then scaled to the range [0, 1] to ensure consistent input representation across all spectral bands.

The full dataset, comprised 2,997 UAV images, acquired at two phenological stages, BBCH73 and BBCH85. Pixel-level annotations were generated for a representative subset of 580 images using the Roboflow platform (Dwyer et al., 2024). The annotated subset was designed to capture variability across phenological stages and illumination conditions, thereby supporting model robustness under differing canopy structures and radiometric scenarios. A multi-class classification scheme was adopted to distinguish the different object categories present in the imagery, including vine canopy, non-canopy elements such as soil and spontaneous vegetation, and background, which comprises shaded areas and other non-informative features. The annotated images were first subdivided into non-overlapping patches of 1600×1300 pixels to standardize spatial units for model development. These annotated patches were then partitioned at image level into training, validation, and independent test subsets using a 70:20:10 ratio to prevent spatial leakage. This partitioning resulted in 406 training images, 116 validation images, and 58 independent test images. To increase the number of training samples and enhance spatial generalization, each 1600×1300 patch was further subdivided into 240×240-pixel tiles using a sliding-window strategy with 67% overlap, corresponding to a stride of approximately 80 pixels. Under this configuration, each image generated 252 tiles. The annotated subset therefore produced 102,312 training tiles, 29,232 validation tiles, and 14,616 test tiles, for a total of 146,160 annotated tiles used for model training and evaluation. To lodge multispectral UAV imagery, the original 7×7 convolutional layer was adapted at the input stage of the network, enabling effective processing of the multi-band reflectance data. This adaptation allowed the model to learn both spectral and spatial features relevant to vineyard canopy delineation. The model was trained using a categorical cross-entropy loss function and optimized with the Adam algorithm with an initial learning rate of 0.001. A softmax activation function was applied at the output layer to perform multi-class pixel-wise classification. Training was conducted with a batch size of 16. The network was trained to perform pixel-wise multi-class classification, assigning each pixel to one of the three defined classes. Although segmentation performance was not the primary objective of this study, its quantitative evaluation ensured the reliability of canopy-derived metrics used in subsequent analyses. The application of the trained model to the complete UAV dataset ensured spatial consistency in canopy extraction across the vineyard, thereby strengthening the reliability of subsequent Fc and canopy NDVI analyses.

The performance of the segmentation model was evaluated on the independent test set using standard pixel-wise classification metrics derived from the confusion matrix. These metrics were selected to assess both spatial agreement and classification reliability across the three target classes. Specifically, class-wise Precision and Recall were computed to quantify the reliability and completeness of canopy detection, respectively. The F1-score was calculated to provide a balanced measure precision and recall. In addition, the Intersection over Union (IoU) was used to evaluate spatial overlap between predicted masks and ground-truth annotations for each class. Mean IoU (mIoU) and macro-averaged Precision (m P_i), Recall (m R_i), and F1-score (mF1) were reported to summarize overall segmentation performance across classes. The detailed accuracy results for all evaluated metrics are provided in the Supplementary Materials in Table S1.

Fc was determined for each meter as geometric ratio between the projected CA and the vineyard block, according to Roma et al. (2025). Subsequently, NDVI was calculated both at the single block scale and at the canopy-only level using the standard formula proposed by Rouse et al. Jr (1974a, b). The resulting values were extracted for statistical assessment, enabling quantitative evaluation of canopy vigour and spatial variability. This structured protocol minimized interference from non-target surfaces while maintaining consistency with state-of-the-art UAV-based viticulture monitoring techniques.

Data analysis

Once the dataset was established, pairwise linear regressions were performed between the yield parameters and the UAV-derived variables to explore their individual relationships. In particular, the correlation between geometric and spectral canopy features. Specifically, pure canopy NDVI and mixed NDVI (soil and canopy) were used as spectral features, while Fc was used as a geometric feature. Subsequently, yield parameters were evaluated against combined spectral–geometric indicators, defined as product terms between NDVI (both canopy-only and block-level) and Fc.

Multiple ML algorithms were implemented using grape yield and RS survey data to perform the yield estimation process in both sampling approaches. A dataset comprising 36 observations was used to train and evaluate four ML models selected based on their documented effectiveness for yield estimation in viticulture: (1) Efficient Linear Model, (2) Support Vector Machine (SVM), (3) Random Forests, representing an ensemble of trees approach, and (4) Gaussian Process Regression (GPR). Five predictors were included: NDVI, canopy-only NDVI, Fc, Fc*NDVI, and Fc*Canopy-only NDVI. Independent modelling sessions were conducted to estimate yield derived from meter-based and vine-based sampling, as well as to compare predictors extracted from RS surveys acquired at BBCH 73 and BBCH 85, respectively. All models were developed using the Statistics and Machine Learning Toolbox in MATLAB environment (The MathWorks, Inc., R2025b). A randomized 5-fold cross-validation procedure was applied to mitigate overfitting risk and ensure robust estimation of model performance, whereby the dataset was randomly partitioned into five equally sized subsets; for each iteration, four subsets were used for training and the remaining subset for validation. All ML models were trained using a consistent hyperparameter scheme to ensure comparability across algorithms. For the efficient linear model, only linear terms were included and the robust fitting option was disabled. The SVM model was trained using a quadratic kernel, with automatic kernel scaling, box constraint, and epsilon selection, and with predictor standardization enabled. GPR was fitted using a constant basis function and an isotropic squared exponential kernel; the kernel scale, signal standard deviation, and sigma were automatically optimized, with predictor standardization enabled. For the random forest model, 30 learners were used, the minimum leaf size was set to 8, and all predictors were considered at each split.

A third modelling framework was then introduced, Bayesian inference modelling, given its dual advantages of being robust and capable of quantifying predictive uncertainty. The Bayesian analyses were performed in the R environment (R Core Team, 2024) using the *brms* package (Bürkner, 2017, 2018), which provides an interface to *Stan* (Carpenter et al., 2017), a probabilistic programming language designed for advanced Bayesian computation. Parameter estimation relied on the Hamiltonian Monte Carlo (HMC) algorithm, a gradient-based Markov Chain Monte Carlo (MCMC) method that improves sampling efficiency and convergence. Specifically, the No-U-Turn Sampler (NUTS), a self-adaptive variant of HMC, was used to automatically tune step sizes and improve convergence for complex model structures (Carpenter et al., 2017; Bürkner, 2017, 2018; Ng'ombe & Lambert, 2021). The response variables modelled were "yield per vine" and "yield per meter". Multiple Bayesian model configurations were tested to evaluate sensitivity to structural assumptions and predictor sets. The chosen covariates included Fc, NDVI at block level and canopy-only

NDVI, derived from vegetation masking. All possible interaction terms among these predictors were considered. Accordingly, the model formula was specified as (Eq. 1):

$$Yield \sim Fc * NDVI * NDVI_{Canopy-only} \tag{1}$$

where the operator * denotes the inclusion of all main effects and their pairwise and three-way interactions according to standard R formula notation. Given the limited availability of similar applications in the literature, standard priors were adopted to ensure model flexibility. Each model was fitted using four MCMC chains, each consisting of 10,000 iterations with 3,000 warm-up samples. Convergence was verified by ensuring all parameters had a Gelman–Rubin statistic ($\hat{R}$) < 1.01 and both bulk and tail effective sample sizes (ESS) exceeded 100 per chain (Vehtari et al., 2021).

Posterior distributions were summarized by reporting the 0.025, 0.50, and 0.975 quantiles, providing median parameter estimates and associated 95% credible intervals. After assessing model adequacy through posterior predictive checks, the best-performing Bayesian model was selected based on Leave-One-Out cross-validation (LOO) estimates and Bayesian R^2 and subsequently applied to generate yield maps.

Model validation was subsequently performed by evaluating predictive performance under real field conditions. Specifically, model outputs at field scale were compared against the total yield measured at harvest, enabling an assessment of predictive accuracy and robustness of the proposed modelling approach.

Performance evaluations

For model comparison, four key metrics were selected: Pearson correlation coefficient (r, Eq. 2), coefficient of determination (R^2, Eq. 3), normalized root mean square error (nRMSE, %, Eq. 4), and normalized mean absolute error (nMAE, %, Eq. 5). To allow model comparison across datasets with different yield units (per vine and per meter), nRMSE and nMAE were normalized by the mean of the observed values and reported as percentages. The metrics were calculated as follows:

$$r = \frac{\Sigma_{i=1}^{n}\left(y_i - \bar{y}\right)\left(\bar{y}_i - \bar{\hat{y}}_i\right)}{\sqrt{\Sigma_{i=1}^{n}\left(y_i - \bar{y}\right)^2 \ \Sigma_{i=1}^{n}\left(\hat{y}_i - \bar{\hat{y}}_i\right)^2}} \tag{2}$$

$$R^2 = 1 - \frac{\Sigma_{i=1}^{n}\left(y_i - \hat{y}_i\right)^2}{\Sigma_{i=1}^{n}\left(y_i - \bar{y}\right)^2} \tag{3}$$

$$nRMSE = 100 * \frac{\sqrt{\frac{1}{n}\ \Sigma_{i=1}^{n}\left(y_i - \hat{y}_i\right)}}{\bar{y}} \tag{4}$$

$$nMAE = 100 * \frac{\left(\frac{1}{n}\ \Sigma_{i=1}^{n}\left|y_i - \hat{y}_i\right|\right)}{\bar{y}} \tag{5}$$

where y_i is the observed value, $\hat{y}_i$ is the predicted value, $\bar{y}$ represents the mean of the observed values and $\bar{\hat{y}}$ is the mean of the predicted values, n is the total number of observations and nRMSE and nMAE are expressed in percentage (%). These metrics provide complementary and interpretable measures of prediction accuracy and model error, allowing a robust comparison among different modelling approaches.

Results

The experimental design enabled a direct comparison between two yield-sampling strategies in VSP-trained vineyards, revealing their influence on model performance across different methodological approaches. The following sections detail the results from the three predictive frameworks and their ability to estimate yield under each sampling approach.

Linear relationships between yield and UAV-derived features

Across both phenological stages, linear regressions revealed consistent positive associations between UAV-derived spectral and geometrical metrics and yield (Figs. 3 and 4; Table 1), confirming the capacity of those features to reflect yield variability in VSP-trained vineyards. A clear difference was observed between the two sampling methods adopted for all the features considered. Scatterplots (Figs. 3 and 4) show consistent positive trends between yield and NDVI, canopy-only NDVI, Fc and their interaction terms, NDVI * Fc and canopy-only NDVI * Fc. Better trends are observed at BBCH 73 compared to BBCH 85. Points

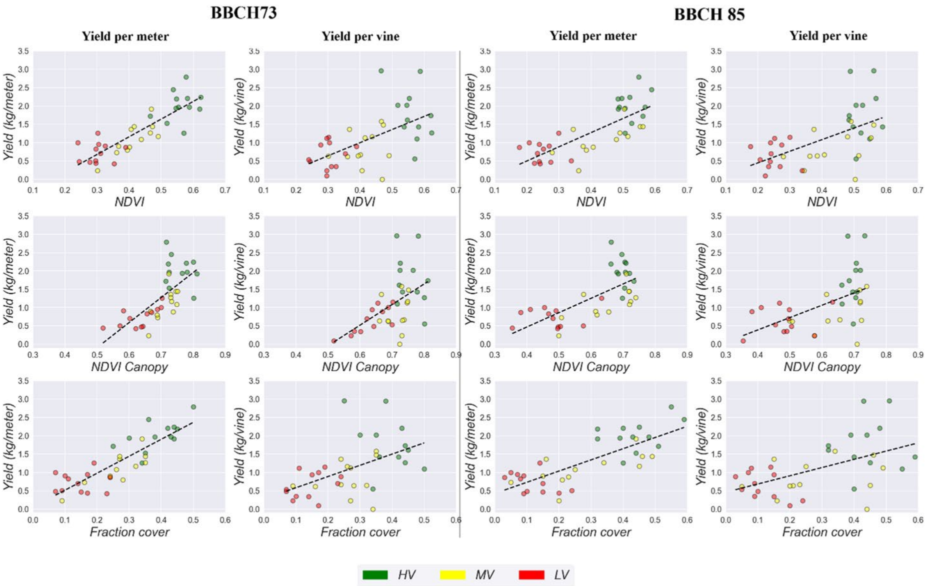

Fig. 3 Relationships between yield and UAV-based features acquired in BBCH 73 and BBCH 85. Scatterplots show the linear regressions between yield per meter and yield per vine against three UAV-derived indicators: NDVI, canopy NDVI, and Fc. Points are coloured according to plot's vigour classes: high vigour (HV, green), medium vigour (MV, yellow), and low vigour (LV, red) (Color figure online)

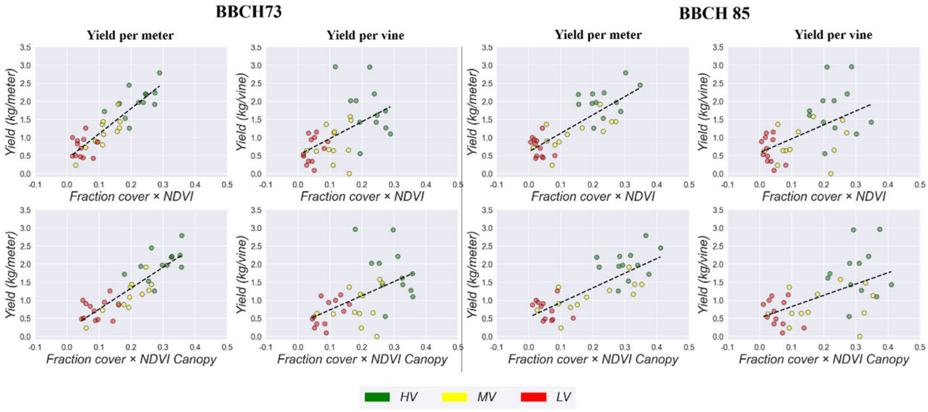

Fig. 4 Relationships between yield and UAV-based combined features acquired in BBCH 73 and 85. Scatterplots show the linear regressions between yield per meter (left column of each pair) and yield per vine (right column of each pair) against two composite vegetation indicators: Fc × NDVI canopy and Fc × NDVI. Points are coloured according to plot's vigour classes: high vigour (HV, green), medium vigour (MV, yellow), and low vigour (LV, red) (Color figure online)

Table 1 Quantitative representation of performance of linear regression between yield and UAV-based features

Feature	Phenological stage	Sampling method	r	R^2	nRMSE (%)	nMAE (%)	Significance
NDVI	BBCH 73	Meter	0.85	0.73	26,18	21,20	***
		Vine	0.58	0.33	53,33	40,20	***
	BBCH 85	Meter	0.77	0.59	32,29	28,35	***
		Vine	0.57	0.33	53,55	42,02	***
NDVI Canopy	BBCH 73	Meter	0.70	0.48	36,19	28,88	***
		Vine	0.52	0.27	55,73	39,36	**
	BBCH 85	Meter	0.69	0.47	36,58	31,07	***
		Vine	0.54	0.29	55,03	40,55	**
Fraction cover	BBCH 73	Meter	0.86	0.73	26,11	21,77	***
		Vine	0.51	0.26	56,00	39,84	**
	BBCH 85	Meter	0.79	0.63	31,67	27,75	***
		Vine	0.55	0.30	55,79	44,44	**
Fraction cover × NDVI	BBCH 73	Meter	0.88	0.78	23,76	19,75	***
		Vine	0.54	0.29	55,16	40,27	**
	BBCH 85	Meter	0.81	0.65	30,21	25,90	***
		Vine	0.56	0.31	54,50	43,54	**
Fraction cover × NDVI Canopy	BBCH 73	Meter	0.86	0.75	25,34	20,85	***
		Vine	0.53	0.28	55,39	38,88	**
	BBCH 85	Meter	0.80	0.63	30,92	27,07	***
		Vine	0.56	0.32	54,51	43,07	**

in high-vigour classes (HV) systematically occupied the upper portion of the yield distribution, whereas low-vigour points (LV) clustered at lower values.

At BBCH 73, meter-based sampling shows tight linear trends for NDVI and Fc, with the smallest error envelopes among single predictors (Fig. 3). This is reflected in the performance metrics reported in Table 1, where both NDVI and Fc reach $R^2 = 0.73$ (nRMSE ≈ 26.15%). NDVI Canopy remains significant but with lower performance. The vine-based sampling is visibly more dispersed for all three predictors, with R^2 ranging between 0.26 and 0.33 and nRMSE ranging between 53.33 and 56.00%.

At BBCH 85, the same trend persists with moderately wider bands (Fig. 3). Per-meter fits remain significant across predictors, with Fc and NDVI again the most compact while NDVI Canopy is the least tight. Per-vine sampled fits panels remain weaker overall (Table 1).

Interaction terms display an overall stronger relationship with yield (Fig. 4; Table 1). In BBCH 73, Fc × NDVI delivers the top performance ($R^2 = 0.78$, nRMSE = 23.76%), exceeding single-predictor NDVI/Fc. At BBCH 85, the ranking is preserved with slightly broader dispersion; meter-based Fc × NDVI reaches $R^2 = 0.65$ (nRMSE = 30.21%), improving on NDVI at the same stage. In contrast, vine-based interaction fits remain modest and closely clustered around $R^2 \approx 0.28$–0.32 with nRMSE ≈ 53.50–55.80%, similar to the corresponding single-predictor results.

Linear regression between number of bunches and UAV-derived features

Across both stages, regressions between number of clusters and UAV features were positive but weaker than for yield, with meter-based fits improving performance compared to vine-based sampling (Fig. 5; Table 2). At BBCH 73, single predictors in meter-based panels showed low correlations: Fc was the strongest among them ($R^2 = 0.25$, nRMSE = 25.89%), while NDVI and NDVI Canopy were lower ($R^2 \approx 0.18$, nRMSE ≈ 27.10%). For vine-based sampling, relations were generally negligible ($R^2 \leq 0.06$; nRMSE ≈ 27–48%; mostly n.s.). At BBCH 85, the pattern persisted (Fig. 5).

Composite indicators showed limited gains over single predictors for number of bunch cluster (Table 2). At BBCH 73, Fc × NDVI and Fc × NDVI Canopy in meter-based sampling achieved $R^2 \approx 0.25$ (nRMSE ≈ 26%). At BBCH 85, composites remained low ($R^2 \approx 0.15$, nRMSE ≈ 27%), and vine-based interactions were largely non-significant (Fig. 6).

Machine learning models performance

Figure 7 shows the results of the comparative performance of the four ML algorithms for yield estimation under the two sampling strategies, meter-based and vine-based, at BBCH 73, which provided the highest predictive accuracy.

Across all algorithms, meter-based sampling outperformed vine-based sampling in all metrics. For the meter-based sampling, metrics result in a narrow, high range ($R^2 = 0.70$–0.76, nRMSE = 25.6–28.7%), while vine-based sampling remained in lower and more dispersed ranges ($R^2 = 0.15$–0.27, nRMSE = 57.0–61.5%). The best scores were obtained by the Efficient Linear and SVM models under meter-based sampling (both $R^2 = 0.76$, nRMSE ≈ 25.7%, nMAE ≈ 21.8%), closely followed by GPR. Under vine-based sampling, none of the algorithms achieved competitive accuracy; SVM and Efficient Linear were marginally higher ($R^2 \approx 0.24$–0.27) than Ensemble and GPR ($R^2 \approx 0.15$–0.17). A similar pattern

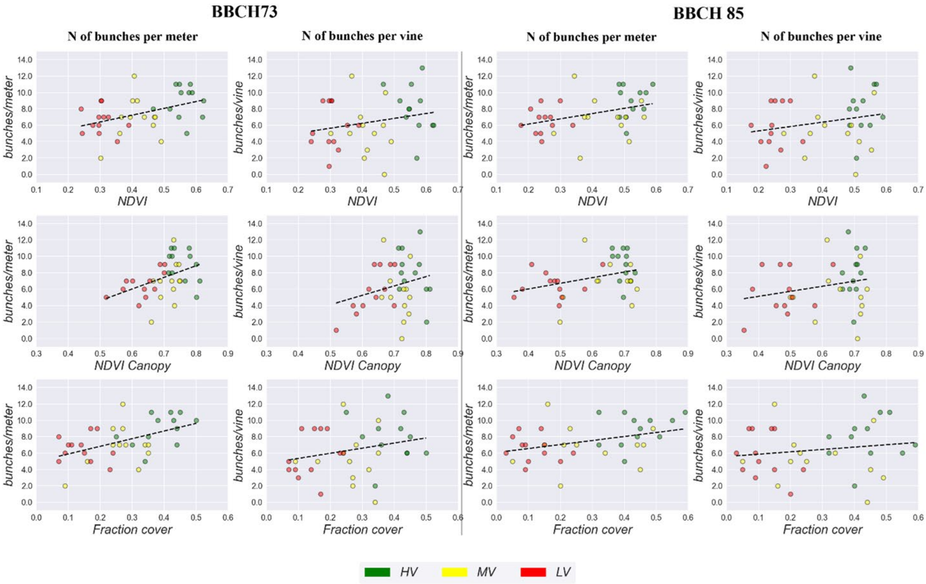

Fig. 5 Relationships between the number of grape clusters and UAV-based features acquired in BBCH 73 and 85. Scatterplots show the linear regressions between the number of grape clusters per meter and per vine against three vegetation indicators: NDVI, canopy NDVI, and Fc. Points are coloured according to plot's vigour classes: high vigour (HV, green), medium vigour (MV, yellow), and low vigour (LV, red) (Color figure online)

was observed at BBCH 85, but with an overall lower predictive performance (Supplementary Materials, Fig. S1).

Performance of Bayesian modelling

Bayesian modelling based on meter-based sampled data and RS features acquired at BBCH 73 showed the strongest predictive performance, with a coefficient of determination R^2 of 0.84, a nRMSE of 20.47% and a nMAE equal to 17.46% (Fig. 8a). The predicted posterior medians and the observed yield values are closely aligned. Most observations cluster symmetrically along the regression line. The uncertainty bar, posterior standard deviations, remain relatively narrow and consistent. Minor deviations are observed at the upper end of the yield distribution, while slight underestimations are present for lower values. Conversely, Bayesian modelling trained using yield data expressed per vine showed substantially lower predictive performance (Fig. 8b). The model achieved an R^2 of 0.41, with an nRMSE of 50.08%. The data points are more dispersed around the 1:1 line, with broader 95% credible intervals. In particular, over- and underestimation patterns are visible at both extremes of the yield range. A similar overall pattern was observed using RS data acquired later in the season, at BBCH 85, although with an observed lower predictive performance (Supplementary Materials, Fig. S2).

Table 2 Quantitative representation of performance of linear regression between the number of grape clusters and UAV-based features

Feature	Phenological stage	Sampling method	*r*	R^2	nRMSE (%)	nMAE (%)	Significance
NDVI	BBCH 73	Meter	0.43	0.18	27,07	21,39	*
		Vine	0.22	0.05	46,92	37,51	n.s.
	BBCH 85	Meter	0.37	0.14	27,80	22,11	*
		Vine	0.22	0.05	46,93	38,17	n.s.
NDVI Canopy	BBCH 73	Meter	0.42	0.18	27,16	21,43	*
		Vine	0.25	0.06	46,67	37,72	n.s.
	BBCH 85	Meter	0.35	0.12	28,02	22,54	*
		Vine	0.23	0.05	46,86	38,05	n.s.
Fraction cover	BBCH 73	Meter	0.50	0.25	25,89	21,00	**
		Vine	0.24	0.06	46,69	36,85	n.s.
	BBCH 85	Meter	0.39	0.15	27,90	21,75	*
		Vine	0.21	0.04	47,56	38,42	n.s.
Fraction cover × NDVI	BBCH 73	Meter	0.49	0.24	26,14	20,77	**
		Vine	0.24	0.06	46,77	37,26	n.s.
	BBCH 85	Meter	0.39	0.15	27,64	21,49	*
		Vine	0.21	0.04	47,28	38,26	n.s.
Fraction cover × NDVI Canopy	BBCH 73	Meter	0.50	0.25	25,90	21,03	**
		Vine	0.24	0.06	46,71	37,01	n.s.
	BBCH 85	Meter	0.38	0.14	27,82	21,81	*
		Vine	0.20	0.04	47,36	38,27	n.s.

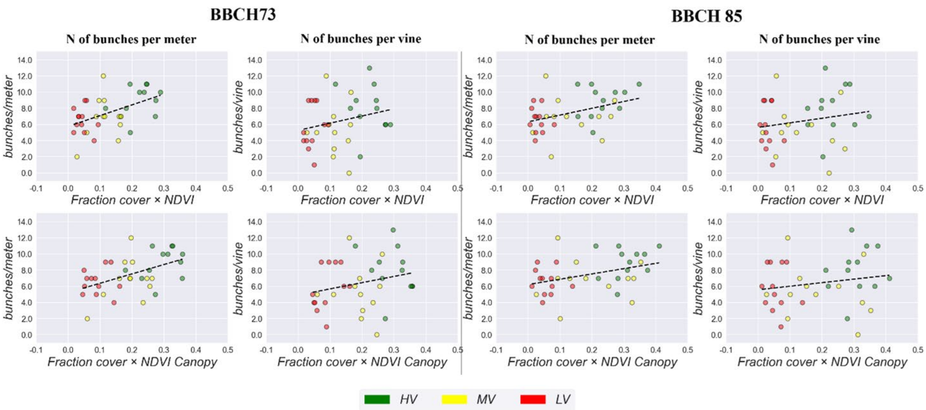

Fig. 6 Relationships between the number of grape clusters and UAV-based combined features acquired in BBCH 73 and 85. Scatterplots show the linear regressions between the number of grape clusters per meter and per vine against two composite vegetation indicators: Fc× NDVI canopy and Fc × NDVI. Points are coloured according to plot's vigour classes: high vigour (HV, green), medium vigour (MV, yellow), and low vigour (LV, red) (Color figure online)

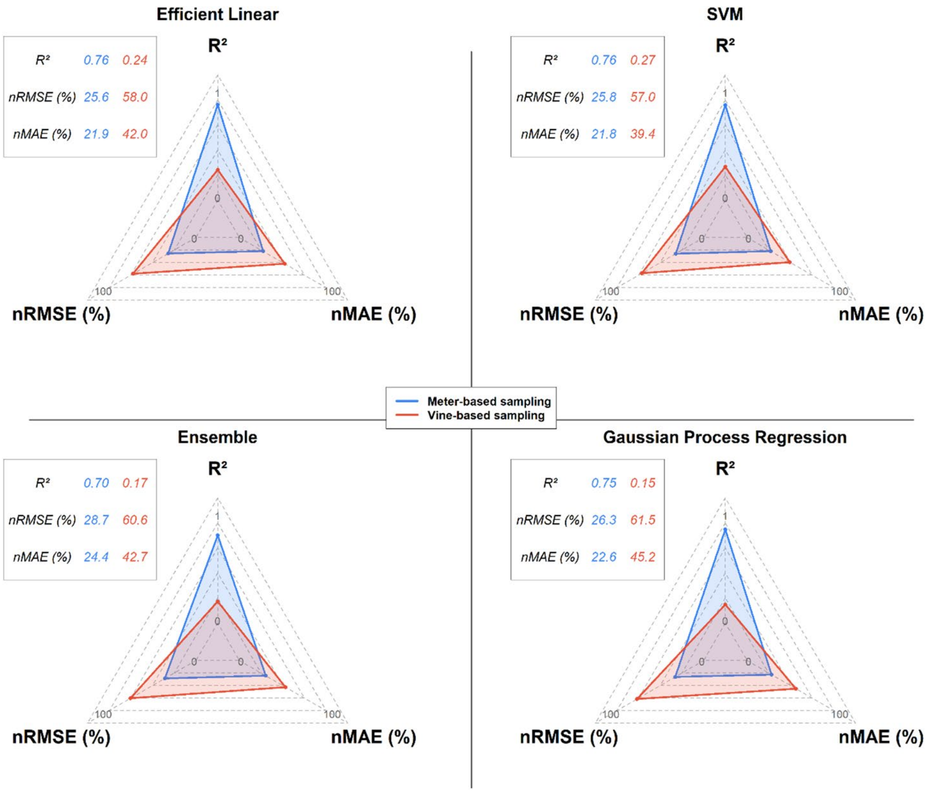

Fig. 7 Comparison between meter-based sampling (blue) and vine-based sampling (red) across the four ML models in BBCH 73: Efficient linear, SVM, ensemble, and GPR. Radar plots display the performance for the evaluated metrics: R², nRMSE and nMAE (Color figure online)

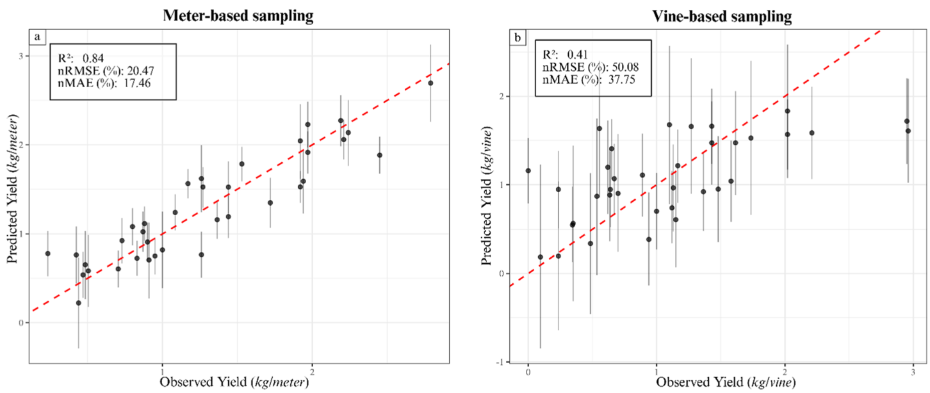

Fig. 8 Observed versus predicted yield values obtained from the Bayesian inference model for yield per meter (kg·m⁻¹) (**a**) and yield per vine (kg·vine⁻¹) (**b**) at BBCH 73. Black dots represent the posterior medians of the predicted yield, with vertical bars indicating the 95% credible intervals. The red dashed line represents the 1:1 relationship. Model performance metrics (R², nRMSE and nMAE) are reported in each panel

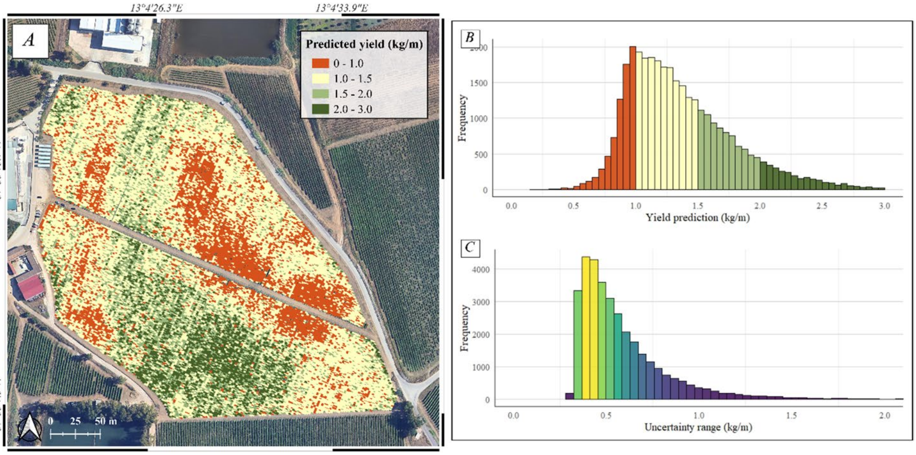

Fig. 9 Spatial distribution of predicted grapevine yield (kg·m^{-1}) across the experimental vineyard (**A**) and corresponding frequency distributions (**B**). Histogram of yield predictions (kg·m^{-1}) highlighting a right-skewed distribution. Histogram of prediction uncertainty (**C**) (kg·m^{-1}), showing that most estimates exhibited low uncertainty (kg·m^{-1})

Spatial variability of yield and uncertainty analysis

The yield prediction map in Fig. 9A revealed marked spatial variability across the vineyard, with estimated values ranging from below 1.0 kg·m^{-1} to over 3 kg·m^{-1}. The highest predicted yields were concentrated in the southern and central-eastern sectors, while lower-yielding zones were predominantly located in the northern portion of the field.

The overall distribution of predicted yield followed a right-skewed pattern (Fig. 9B) with a dominant class between 1.0 and 1.5 kg·m^{-1}. The uncertainty analysis (Fig. 9C) indicates that most predictions exhibited an uncertainty below 0.6 kg·m^{-1}, confirming a satisfactory model reliability at the intra-vineyard scale. The observed yield of the experimental vineyard was 6.54 t·ha^{-1}, corresponding to an average of 1.43 kg·vine^{-1}. Among the two sampling strategies evaluated, the meter-based sampling approach provided a more accurate estimation of yield per hectare than the vine-based method. Specifically, the meter-based sampling underestimated the actual yield by only 5.41%, predicting 6.19 t·ha^{-1} (1.36 kg·vine^{-1}), whereas the vine-based method underestimated the total yield by 17.6%, corresponding 5.39 t·ha^{-1} (1.18 kg·vine^{-1}).

Discussions

The findings show that the definition of the ground-truth unit markedly conditions the accuracy of RS-based yield modelling in VSP vineyards. Across simple linear fits, ML and Bayesian models, the meter-based sampled data outperformed the vine-based sampling approach, with consistently higher R^2 and lower errors. The one-meter segments preserve the geometric continuity of the canopy wall and align better with the UAV-ground projection. This reduces the effects of edge overlap and systematic misalignment that occur when a single grapevine is treated as an isolated unit and subsequently associated with RS data.

The meter-based method reflects spatial continuity in VSP systems more accurately, since the canopy is a continuous productive unit rather than a discrete system of individual vines. In this study, ~ 25% of the recorded yield was associated with vine-based segments that did not align with the corresponding meter-based units. This indicates that a substantial portion of production originated from canopy portions geometrically inconsistent with the 2D footprint of RS data, providing quantitative evidence of the mismatch inherent to vine-based sampling.

The results obtained in this study address a key methodological limitation previously identified in UAV-based vineyard yield estimation. Earlier research demonstrated the potential of RS imagery to predict yield with high accuracy. However, these studies relied predominantly on vine-based ground-truth data, which inherently limits model generalization across different training systems and canopy architectures (Di Gennaro et al. 2019b; Ballesteros et al. 2020a; López-García et al. 2022). In vine-level sampling, the predictive relationship between RS canopy descriptors and actual yield is strongly influenced by pruning configuration, vine geometry, and canopy discontinuity, all of which vary considerably between vineyards (Keller et al., 2010; Carrillo et al., 2016; Gatti et al., 2017).

In this study the bivariate analyses showed that, for meter-based sampled data, yield was strictly related to canopy geometry and spectral response. Composite predictors such as Fc × NDVI and Fc × NDVI canopy provided the best results, with more noticeable gains earlier in the season (BBCH 73), when canopies have already reached maximum vegetative growth. Meanwhile, the weak relationships observed for the number of grape clusters suggest the presence of complex physiological mechanisms controlling vine cluster size that are not fully detectable by RS alone. These findings align with prior evidence that fusing geometric and spectral features improves predictive power for functional relationships with yield and other parameters (Ballesteros et al. 2020b); in another example, Campos et al. (2021b) reported improvements when NDVI was combined with a canopy-projection metric (their analogue of Fc) to relate RS to canopy volume.

The results obtained in this study help to provide context since data referring to individual vines often show strong correlations, despite the high geometric misalignments likely in VSP systems. In fact, some studies did not perform validation at the individual vine level, but aggregated vines into short sections or plots to suppress sampling errors. For example, Carrillo et al. (2016); Ballesteros et al. (2020b) aggregated five consecutive vines and plots of ~ 18 vines, respectively, into a single sampling unit. In line with this basis, in a previous analysis, the authors compared sampling per vine with contiguous blocks of six vines and found that the block strategy was more accurate and less prone to bias (Canicattì et al. 2025b). Others approaches compare a "representative" vine to plot-level RS features (López-García et al., 2022). While effective, these strategies do not fully take the advantage of UAV spatial resolution and increase ground effort, as large numbers of vines should be harvested or counted to stabilize the signal.

ML outcomes corroborate a model-agnostic benefit for the meter-based sampling design. Across distinct algorithmic families, meter-based ground truth yielded systematically higher R^2 and lower nRMSE/nMAE than per-vine sampling, indicating that the improvement derives from reduced label noise via better footprint congruence, rather than any algorithm-specific effect. These patterns are consistent with those in Matese and Di Gennaro (2021), showing that coupling NDVI with canopy thickness (a geometric descriptor similar to Fc) improved fits; in a 5-fold cross-validation comparison, Random Forest performed best (approximately $R^2 \approx 0.73$ with spectral+geometric inputs), with most algorithms in the $R^2 \approx 0.65–0.70$ range.

The Bayesian posterior results highlighted a clear gap between yield per meter ($R^2 \approx 0.83$; nRMSE ≈ 20.5%; narrow credible intervals) and yield per vine ($R^2 \approx 0.41$; nRMSE ≈ 50.0%; wider intervals), reinforcing that the meter-based unit reduces observation noise and propagates less uncertainty. From a modelling perspective, yield per meter enhances the structural coherence between field and RS data, improving the capacity of Bayesian modelling frameworks to capture spatial dependencies and reduce posterior uncertainty. The resulting models exhibit smoother and more consistent predictive behaviour across different vigour zones and canopy densities. Compared to the other study on Bayesian yield mapping reported in Canicattì et al. (2025b) the meter-based method tested in this study increases the spatial resolution of the prediction, reaching one meter resolution, a very useful information in all the condition were high performance evaluation is needed, like in plot experiment or in fragmented agricultural situations. Validation against total field production confirmed the generalizability of the findings. A more robust and transferable sampling framework that mitigates the geometric biases of vine-based protocols may also accelerate the broader adoption of PV (Santesteban et al., 2013). Taken together, these findings contribute to closing an existing research gap by demonstrating that the sampling unit itself plays a pivotal role in the reliability and generalization of UAV-based yield models.

Limitations and future prospectives

The framework presented in this study demonstrated good capabilities for improving yield mapping in VSP vineyards using UAV multispectral data. Nevertheless, some limitations persist, alongside numerous avenues for future development.

This work should be interpreted primarily as a methodological validation study. Its main contribution is to assess how the definition of the ground-truth unit (vine- vs. meter-based) conditions RS–yield relationships in VSP vineyards, with the aim of supporting best practices in ground-truth collection in PV. To keep the comparison focused on the "sampling unit effect", a simplified predictor set was adopted. In particular were used Fc as geometric and NDVI as spectral descriptors of crop status. This choice was motivated by the need for an interpretable and widely used proxy of canopy vigour and crop productivity; however, the inclusion of additional VIs (e.g. GNDVI, NDRE, OSAVI) and/or multi-band combinations may improve predictive performance and should be explored in future work.

The generalizability of the findings is also bounded by the experimental domain. Trials were conducted within a single experimental field, while the relationships between spectral/geometric predictors and yield are physiologically sensitive to architectural features, trunk height, cordon height, row spacing, canopy thickness, pruning style. Those field condition modulate the pixel-scale thickness of canopy and background and, hence, the resulting spectral signal. Notwithstanding these constraints, the meter-based sampling showed consistent gains over vine-based sampling across linear, ML, and Bayesian frameworks, indicating that the geometric rationale behind the meter-based unit reduces sampling bias and improves generalizability. Still, this study's aim does not claim a universal predictor; rather, it provides a sampling protocol that improves accuracy and correctness of RS-based yield estimation.

Future work should extend this validation across broader experimental trials through multi-variety, multi-region, and multi-year experiments, and explicitly test alternative wall-trained systems beyond grapevine, including super-high-density (SHD) olives, apple fruiting walls, and other hedgerow orchards. These expanded datasets would also enable the integration of 3D structural descriptors (e.g., height, porosity, volume from LiDAR) with spectral predictors, to further improve transferability and predictive performance. Methodologically, a Bayesian hierarchical framework could be next step to pool across genotype, training system, site, and year, while accommodating spatial effects and quantifying the uncertainty; this would allow principled sharing of information across trials, potentially reducing the number of calibration points in new trials. Finally, the meter-based sampling logic should be evaluated for other targets beyond yield, like biomass, pruning weight, LAI, or nitrogen status, to test whether the same geometric alignment consistently improves functional relationships across traits and phenological stages.

Conclusions

The results of this research demonstrate that the choice of ground-truth method is a first-order driver of accuracy in RS-based yield modelling in VSP-trained vineyards. From ground sampling that delimits contiguous meter-based segments rather than individual grape vines, it has been possible to systematically improve performance on tested models, showing higher R^2 values. Meter-based sampling preserves the geometric continuity of the canopy wall characteristic of VSP systems, whereas vine-level units introduce misalignment and geometric bias. Bivariate analyses confirmed that yield relates tightly to canopy features, with composite geometric/spectral predictors performing best, especially at BBCH 73. Bayesian inference further quantified the gain of yield per meter sampling method, and whole-field yield totals corroborated external validity. While these findings were obtained in VSP vineyards, future research should test transferability to alternative training systems, environments and cultivars. Overall, redefining the reference unit as contiguous canopy segments provides a sampling framework that systematically improves the accuracy and robustness of UAV-based yield models and enables their use in the PV sector.

Supplementary Information The online version contains supplementary material available at https://doi.org/10.1007/s11119-026-10391-0.

Author contributions Marco Canicattì: Conceptualization, Methodology, Software, Data Curation, Writing -Original Draft; Pietro Catania: Supervision, Investigation, Methodology, Validation, Review & Editing; Eliseo Roma: Data Curation, Writing - Review & Editing; Salvatore Amato: Validation, Writing - Review & Editing; Massimo Vincenzo Ferro: Data Curation, Methodology, Software, Validation, Writing -Original Draft Writing - Review & Editing; Mariangela Vallone: Supervision, Methodology, Validation, Review & Editing; Santo Orlando: Supervision, Investigation, Validation, Review & Editing;

Funding Open access funding provided by Università degli Studi di Palermo within the CRUI-CARE Agreement.

Data availability The datasets analyzed in thisstudy are available on request from the corresponding author.

Declarations

Competing interests The authors declare no competing interests.

References

Acevedo-Opazo, C., Tisseyre, B., Ojeda, H., & Guillaume, S. (2010). Spatial extrapolation of the vine (Vitis vinifera L.) water status: A first step towards a spatial prediction model. *Irrigation Science*, *28*, 143–155.

Araya-Alman, M., Leroux, C., Acevedo-Opazo, C., et al. (2019). A new localized sampling method to improve grape yield estimation of the current season using yield historical data. *Precision Agriculture*, *20*, 445–459. https://doi.org/10.1007/s11119-019-09644-y

Ballesteros, R., Intrigliolo, D. S., Ortega, J. F., et al. (2020a). Vineyard yield estimation by combining remote sensing, computer vision and artificial neural network techniques. *Precision Agriculture*, *21*, 1242–1262.

Ballesteros, R., Intrigliolo, D. S., Ortega, J. F., et al. (2020b). Vineyard yield estimation by combining remote sensing, computer vision and artificial neural network techniques. *Precision Agriculture, 21*, 1242–1262. https://doi.org/10.1007/s11119-020-09717-3

Bannari, A., Morin, D., Bonn, F., & Huete, A. (1995). A review of vegetation indices. *Remote Sensing Reviews, 13*, 95–120.

Berry, A., Vivier, M., & Poblete-Echeverría, C. (2024). Evaluation of canopy fraction-based vegetation indices, derived from multispectral UAV imagery, to map water status variability in a commercial vineyard. *Irrigation Science,* (1), 19. https://doi.org/10.1007/s00271-023-00907-1

Biglia, A., Zaman, S., Gay, P., et al. (2022). 3D point cloud density-based segmentation for vine rows detection and localisation. *Computers and Electronics in Agriculture, 199*, Article 107166.

Bollas, N., Kokinou, E., & Polychronos, V. (2021). Comparison of sentinel-2 and UAV multispectral data for use in precision agriculture: An application from northern greece. *Drones*, *5*, 35.

Bramley, R., & Hamilton, R. (2004). Understanding variability in winegrape production systems: 1. Within vineyard variation in yield over several vintages. *Australian Journal of Grape and Wine Research*, *10*, 32–45.

Bürkner, P-C. (2017). brms: An R Package for Bayesian Multilevel Models Using Stan. *Journal of Statistical Software*, *80*, 1–28. https://doi.org/10.18637/jss.v080.i01

Bürkner, P-C. (2018). Advanced Bayesian Multilevel Modeling with the R Package brms. *The R Journal*, *10*, 395–411.

Campos, I., Neale, C. M., López, M-L., et al. (2014). Analyzing the effect of shadow on the relationship between ground cover and vegetation indices by using spectral mixture and radiative transfer models. *Journal of Applied Remote Sensing*, *8*, 083562–083562.

Campos, J., García-Ruíz, F., & Gil, E. (2021a). Assessment of vineyard canopy characteristics from vigour maps obtained using UAV and satellite imagery. *Sensors, 21*, Article 2363.

Campos, J., García-Ruíz, F., & Gil, E. (2021b). Assessment of vineyard canopy characteristics from vigour maps obtained using UAV and satellite imagery. *Sensors, 21*, Article 2363. https://doi.org/10.3390/s21072363

Canicattì, M., & Vallone, M. (2024). Drones in vegetable crops: A systematic literature review. *Smart Agricultural Technology*. https://doi.org/10.1016/j.atech.2024.100396

Canicattì, M., Catania, P., & Ferro, M. V. (2025). Sustainable Soil Management in Viticulture: A Case Study. In L. Sartori, P. Tarolli, & L. Guerrini (Eds.), *Biosystems Engineering Promoting Resilience to Climate Change - AIIA 2024 - Mid-Term Conference* (pp. 816–823). Springer Nature Switzerland.

Canicattì, M., Ferro, M. V., Vallone, M., et al. (2025b). Bayesian yield mapping and uncertainty analysis in vineyards using remote sensing data and grape harvester tracking. *Precision Agric, 26*, 1–35. https://doi.org/10.1007/s11119-025-10258-w

Carpenter, B., Gelman, A., Hoffman, M. D., et al. (2017). Stan: A probabilistic programming language. *Journal of Statistical Software, 76*, 1–32. https://doi.org/10.18637/jss.v076.i01

Carrillo, E., Matese, A., Rousseau, J., & Tisseyre, B. (2016). Use of multi-spectral airborne imagery to improve yield sampling in viticulture. *Precision Agriculture*, *17*, 74–92. https://doi.org/10.1007/s11119-015-9407-8

Catania, P., Ferro, M. V., Roma, E., et al. (2023aa). Evaluation of Different Flight Courses with UAV in Vineyard. *Springer,* 457–467. https://doi.org/10.1007/978-3-031-30329-6_47

Catania, P., Roma, E., Orlando, S., & Vallone, M. (2023b). Evaluation of Multispectral Data Acquired from UAV Platform in Olive Orchard. *Horticulturae*, *9*, 133.

Cinat, P., Di Gennaro, S. F., Berton, A., & Matese, A. (2019). Comparison of unsupervised algorithms for vineyard canopy segmentation from UAV multispectral images. *Remote Sensing, 11*, Article 1023.

Clingeleffer, P. R., & Krstic, M. (2003). *Crop development, crop estimation and crop control to secure quality and production of major wine grape varieties: A national approach: Final report to Grape and Wine Research & Development Corporation*. Grape and Wine Research & Development Corporation.

Comba, L., Biglia, A., Ricauda Aimonino, D., et al. (2020). Leaf Area Index evaluation in vineyards using 3D point clouds from UAV imagery. *Precision Agriculture*, *21*, 881–896.

de la Fuente, M., Linares, R., Baeza, P., et al. (2015). Comparison of different methods of grapevine yield prediction in the time window between fruitset and veraison. *OENO One, 49*, 27–35. https://doi.org/10.20870/oeno-one.2015.49.1.96

Di Gennaro, S. F., Dainelli, R., Palliotti, A., et al. (2019a). Sentinel-2 validation for spatial variability assessment in overhead trellis system viticulture versus UAV and agronomic data. *Remote Sensing, 11*, Article 2573.

Di Gennaro, S. F., Toscano, P., Cinat, P., et al. (2019b). A Low-Cost and Unsupervised Image Recognition Methodology for Yield Estimation in a Vineyard. *Frontiers In Plant Science, 10*,. https://doi.org/10.3389/fpls.2019.00559

Dwyer, B., Nelson, J., & Solawetz, J. (2024). ea Roboflow (version 1.0)[software]. computer vision.

Ferro, M. V., Catania, P., Miccichè, D., et al. (2023a). Assessment of vineyard vigour and yield spatio-temporal variability based on UAV high resolution multispectral images. *biosystems engineering*, *231*, 36–56.

Ferro, M. V., Catania, P., Miccichè, D., et al. (2023b). Assessment of vineyard vigour and yield spatio-temporal variability based on UAV high resolution multispectral images. *Biosystems Engineering*, *231*, 36–56. https://doi.org/10.1016/j.biosystemseng.2023.06.001

Ferro, M. V., Sørensen, C. G., & Catania, P. (2024). Comparison of different computer vision methods for vineyard canopy detection using UAV multispectral images. *Computers and Electronics in Agriculture, 225*, Article 109277.

Gao, L., Wang, X., Johnson, B. A., et al. (2020). Remote sensing algorithms for estimation of fractional vegetation cover using pure vegetation index values: A review. *ISPRS Journal of Photogrammetry and Remote Sensing, 159*, 364–377.

Gatti, M., Garavani, A., Vercesi, A., & Poni, S. (2017). Ground-truthing of remotely sensed within-field variability in a cv. Barbera plot for improving vineyard management. *Australian journal of grape and wine research*, *23*, 399–408.

Guilpart, N., Metay, A., & Gary, C. (2014). Grapevine bud fertility and number of berries per bunch are determined by water and nitrogen stress around flowering in the previous year. *European Journal of Agronomy*, *54*, 9–20.

Hossain, M. D., & Chen, D. (2019). Segmentation for Object-Based Image Analysis (OBIA): A review of algorithms and challenges from remote sensing perspective. *ISPRS Journal of Photogrammetry and Remote Sensing*, *150*, 115–134.

Júnior, A. F. N., Amorim, L., Savary, S., & Willocquet, L. (2018). Modelling the dynamics of grapevine growth over years. *Ecological Modelling, 369*, 77–87.

Keller, M., Tarara, J., & Mills, L. (2010). Spring temperatures alter reproductive development in grapevines. *Australian Journal of Grape and Wine Research*, *16*, 445–454.

Khaliq, A., Comba, L., Biglia, A., et al. (2019). Comparison of satellite and UAV-based multispectral imagery for vineyard variability assessment. *Remote Sensing, 11*, Article 436.

Köppen, W. (1936). Das geographische System der Klimate. 1–44, Berlin (Germany) Gebrüder Borntraeger Present and future Köppen-Geiger Climate Classification Maps at 1-km Resolution. - References - Scientific Research Publishing. https://www.scirp.org/reference/referencespapers?referenceid=3511591. Accessed 18 Feb 2026.

Laurent, C., Oger, B., Taylor, J. A., et al. (2021). A review of the issues, methods and perspectives for yield estimation, prediction and forecasting in viticulture. *European Journal of Agronomy, 130*, Article 126339. https://doi.org/10.1016/j.eja.2021.126339

Leolini, L., Bregaglio, S., Ginaldi, F., et al. (2023). Use of remote sensing-derived fPAR data in a grapevine simulation model for estimating vine biomass accumulation and yield variability at sub-field level. *Precision Agriculture*, *24*, 705–726.

López-García, P., Ortega, J. F., Pérez-Álvarez, E. P., et al. (2022). Yield estimations in a vineyard based on high-resolution spatial imagery acquired by a UAV. *Biosystems Engineering, 224*, 227–245. https://doi.org/10.1016/j.biosystemseng.2022.10.015

Matese, A., & Di Gennaro, S. F. (2015). Technology in precision viticulture: A state of the art review. *International Journal of Wine Research, 7*, 69–81.

Matese, A., & Di Gennaro, S. F. (2021). Beyond the traditional NDVI index as a key factor to mainstream the use of UAV in precision viticulture. *Scientific Reports, 11*, Article 2721. https://doi.org/10.1038/s41598-021-81652-3

Matese, A., Di Gennaro, S., Miranda, C., et al. (2017). Evaluation of spectral-based and canopy-based vegetation indices from UAV and Sentinel 2 images to assess spatial variability and ground vine parameters. *Advances in Animal Biosciences, 8*, 817–822. https://doi.org/10.1017/S2040470017000929

Meyers, J. M., & Vanden Heuvel, J. E. (2014). Use of normalized difference vegetation index images to optimize vineyard sampling protocols. *American Journal of Enology and Viticulture, 65*, 250–253.

Meyers, J. M., Sacks, G. L., van Es, H. M., & Vanden Heuvel, J. E. (2011). Improving vineyard sampling efficiency via dynamic spatially explicit optimisation. *Australian Journal of Grape and Wine Research, 17*, 306–315.

Mogili, U. R., & Deepak, B. (2018). Review on application of drone systems in precision agriculture. *Procedia computer science*, *133*, 502–509.

Ng'ombe, J. N., & Lambert, D. M. (2021). Using Hamiltonian Monte Carlo via Stan to estimate crop input response functions with stochastic plateaus. *Journal of Agriculture and Food Research, 6*, Article 100226. https://doi.org/10.1016/j.jafr.2021.100226

Pádua, L., Matese, A., Di Gennaro, S. F., et al. (2022). Vineyard classification using OBIA on UAV-based RGB and multispectral data: A case study in different wine regions. *Computers and Electronics in Agriculture, 196*, Article 106905. https://doi.org/10.1016/j.compag.2022.106905

Paszke, A., Gross, S., Massa, F. (2019). PyTorch: an imperative style, high-performance deep learning library. In: Proceedings of the 33rd International Conference on Neural Information Processing Systems. Curran Associates Inc., Red Hook, NY, USA, pp 8026–8037.

QGIS Development Team (2023). QGIS Geographic Information System.

R Core Team (2024). R: A language and environment for statistical computing.

Roma, E., Orlando, S., Carella, A., et al. (2025). Fraction cover estimation using drone-based multispectral images in six olive cultivars and different planting systems: A case study in Sicily. *Smart Agricultural Technology*. https://doi.org/10.1016/j.atech.2025.101323

RouseJr, J., Haas, R. H., Deering, D. (1974a). Monitoring the vernal advancement and retrogradation (green wave effect) of natural vegetation.

Rouse, J. W., Haas, R. H., Schell, J. A. (1974b). Monitoring the vernal advancement and retrogradation (green wave effect) of natural vegetation. NASA/GSFC Type III Final Report, Greenbelt, Md 371.

Santesteban, L. G., Guillaume, S., Royo, J. B., & Tisseyre, B. (2013). Are precision agriculture tools and methods relevant at the whole-vineyard scale? *Precision Agriculture, 14*, 2–17. https://doi.org/10.1007/s11119-012-9268-3

Schoedl, K., Lawo, J., Astutiningsih, N., & Forneck, A. (2012). An experimental design applied to vineyards for identifying spatially and temporally variable crop parameters. *Vitis*, *51*, 53–60.

Squeri, C., Poni, S., Di Gennaro, S. F., et al. (2021). Comparison and ground truthing of different remote and proximal sensing platforms to characterize variability in a hedgerow-trained vineyard. *Remote Sensing, 13*, Article 2056. https://doi.org/10.3390/rs13112056

Towers, P. C., & Poblete-Echeverría, C. (2021). Effect of the illumination angle on NDVI data composed of mixed surface values obtained over vertical-shoot-positioned vineyards. *Remote Sensing, 13*, Article 855.

Valente, D. S. M., Pereira, G. W., de Queiroz, D. M., et al. (2024). Accuracy of various sampling techniques for precision agriculture: A case study in Brazil. *Agriculture, 14*, Article 2198. https://doi.org/10.3390/agriculture14122198

Vehtari, A., Gelman, A., Simpson, D., et al. (2021). Rank-normalization, folding, and localization: An improved Rˆ for assessing convergence of MCMC (with discussion). *Bayesian Analysis, 16*, 667–718. https://doi.org/10.1214/20-BA1221

Xie, Q., Huang, W., Liang, D., et al. (2014). Leaf area index estimation using vegetation indices derived from airborne hyperspectral images in winter wheat. *IEEE Journal of Selected Topics in Applied Earth Observations and Remote Sensing, 7*, 3586–3594.

Authors and Affiliations

Marco Canicattì[1,2] · Pietro Catania[1] · Eliseo Roma[1] · Salvatore Amato[1] · Massimo Vincenzo Ferro[1] · Mariangela Vallone[1] · Santo Orlando[1]

✉ Massimo Vincenzo Ferro
massimovincenzo.ferro@unipa.it

1 Department of Agricultural, Food and Forest Sciences (SAAF), University of Palermo, Viale delle Scienze ed. 4, Palermo 90128, Italy

2 Department of Agroecology, Aarhus University, Blichers Allé 20, Tjele 8830, Denmark